



Article

Predicting Antigenic Peptides from Rocio Virus NS1 Protein for Immunodiagnostic Testing Using Immunoinformatics and Molecular Dynamics Simulation

Marielena Vogel Saivish ^{1,2,†}, Gabriela de Lima Menezes ^{3,4,†}, Vivaldo Gomes da Costa ⁵,
Gislaine Celestino Dutra da Silva ¹, Rafael Elias Marques ², Maurício Lacerda Nogueira ^{1,*} and
Roosevelt Alves Da Silva ^{3,*}

¹ Departamento de Doenças Dermatológicas, Infeciosas e Parasitárias, Faculdade de Medicina de São José do Rio Preto (FAMERP), São José do Rio Preto 15090-000, SP, Brazil; marielenasaivish@gmail.com (M.V.S.); gislaine.cds@gmail.com (G.C.D.d.S.)

² Laboratório Nacional de Biociências, Centro Nacional de Pesquisa em Energia e Materiais (CNPEM), Campinas 13083-100, SP, Brazil; rafael.marques@lnbio.cnpem.br

³ Núcleo Colaborativo de Biosistemas, Universidade Federal de Jataí, Jataí 75801-615, GO, Brazil; gabrieladelima@hotmail.com

⁴ Bioinformatics Multidisciplinary Environment, Programa de Pós Graduação em Bioinformática, Universidade Federal do Rio Grande do Norte, Natal 59078-400, RN, Brazil

⁵ Instituto de Biociências, Letras e Ciências Exatas, Universidade Estadual Paulista (UNESP), São José do Rio Preto 15054-000, SP, Brazil; vivbiom@gmail.com

* Correspondence: mauricio.nogueira@edu.famerp.br (M.L.N.); rooseveltfsicaufg@gmail.com (R.A.D.S.)

† These authors contributed equally to this work.



Citation: Saivish, M.V.; Menezes, G.d.L.; Costa, V.G.d.; Silva, G.C.D.d.; Marques, R.E.; Nogueira, M.L.; Silva, R.A.D. Predicting Antigenic Peptides from Rocio Virus NS1 Protein for Immunodiagnostic Testing Using Immunoinformatics and Molecular Dynamics Simulation. *Int. J. Mol. Sci.* **2022**, *23*, 7681. <https://doi.org/10.3390/ijms23147681>

Academic Editor: Denis Sereno

Received: 20 June 2022

Accepted: 6 July 2022

Published: 12 July 2022

Publisher's Note: MDPI stays neutral with regard to jurisdictional claims in published maps and institutional affiliations.



Copyright: © 2022 by the authors. Licensee MDPI, Basel, Switzerland. This article is an open access article distributed under the terms and conditions of the Creative Commons Attribution (CC BY) license (<https://creativecommons.org/licenses/by/4.0/>).

Abstract: The mosquito-borne disease caused by the Rocio virus is a neglected threat, and new immune inputs for serological testing are urgently required for diagnosis in low-resource settings and epidemiological surveillance. We used in silico approaches to identify a specific antigenic peptide (p_ROCV2) in the NS1 protein of the Rocio virus that was theoretically predicted to be stable and exposed on its surface, where it demonstrated key properties allowing it to interact with antibodies. These findings related to the molecular dynamics of this peptide provide important insights for advancing diagnostic platforms and investigating therapeutic alternatives.

Keywords: antigenic epitopes; Rocio virus; immunodiagnostics; nonstructural protein; linear B-cell epitope prediction

1. Introduction

The recent novel coronavirus (SARS-CoV-2) identified in late 2019 renewed vigilance among the scientific community concerning the emergence and re-emergence of viral diseases. Rocio virus (ROCV) is a potentially emergent virus that was first isolated in 1975 during an outbreak of meningoencephalitis in São Paulo, Brazil; during this period (1975–1977), lethality and permanent sequelae rates of 10% and 20% were reported, respectively [1].

ROCV is a mosquito-borne flavivirus and a human pathogen [2]. The virus is native to Brazil and the vast majority of ROCV infections are thought to be subclinical, with clinical manifestations ranging from uncomplicated fever to fatal meningoencephalitis [2,3]. Birds are the natural reservoir and amplification hosts, and ROCV is maintained in nature in a mosquito–bird–mosquito transmission cycle primarily involving *Psorophora ferox* mosquitoes [4,5]. Serological evidence indicates that this virus circulated in Bahia in the 1990s, and more recently antibodies were observed in horses in the northeast, center-west, and southeast regions of the country [6–8]. Furthermore, during the 2011–2013 DENV outbreak in Goiânia, viral RNA of ROCV was detected in patients with suspected DENV infection [3]. These findings call

attention to the need for broad and constant surveillance for neglected ROCV infections, which in turn requires the development of accurate methods for diagnostics and prevention.

Structurally, ROCV is a spherical virus approximately 50 nm in size with a lipoprotein envelope [9] and genetic material comprising a single strand of positive RNA containing approximately 11 kilobases [10]. This genome is initially translated into large precursor polyproteins that are further processed by viral and host proteases into three structural proteins (C, prM/M, and E) and seven non-structural proteins (NS1, NS2A, NS2B, NS3, NS4A, NS4B, and NS5) [2].

Non-structural protein 1 (NS1) has no enzymatic functions but plays important roles in the pathogenesis of the virus, inside and outside the cell. Specific studies on the exact functions of the NS1 of the ROCV are still lacking, but its role has been widely reported for viruses of the same genus. When in the cell membrane or the extracellular environment, NS1 can antagonize or modify the functions of the proteins of the complement system, affecting the performance of the host's immune system [11–13]. In the intracellular environment, NS1 remodels the structure of the endoplasmic reticulum and interacts with the surface of the virion, fundamental steps for RNA replication and production of infective viral particles [14,15]. However, further studies specifically involving the ROCV NS1 should be performed to clarify its role in the intracellular environment, cell membrane, and extracellular environment.

Once circulating in the plasma, the NS1 protein is an excellent target for diagnostic tests; in fact, rapid diagnostic tests and enzyme-linked immunosorbent assays (ELISA) are broadly used to detect NS1 for Dengue virus (DENV) and Zika virus (ZIKV), and many studies have also examined its use in diagnosing other flaviviruses [16–21]. Rapid diagnostic tests are cheap, easy to use, and do not require specialized laboratory structures, which is important in low-income regions. However, to our knowledge, no diagnostic tests exist for ROCV. Synthetic peptides have recently emerged as novel targets for efficient serological diagnosis of infectious viral, bacterial, and parasitic diseases [22–29]. Such molecules could be applied in rapid diagnostic tests or other immunodiagnostic platforms such as ELISA to diagnose acute ROCV infection, offering lower production costs, higher specificity and reproducibility with no variation between batches, and larger-scale production compared to diagnosis based on whole antigens [30]. However, accurate identification of more immunodominant epitopes is still required, and this study consequently identified B-cell epitopes from ROCV NS1 *in silico* and proposed a peptide for application in immunodiagnostic tests for ROCV.

2. Results

2.1. ROCV NS1 Has High Amino Acid Identity with Other Flaviviruses

The homology of amino acid identity was analyzed to identify the presence of unique amino acid regions of ROCV NS1. The alignment showed that the NS1 protein sequences of ROCV strains are conserved and that there are important variations in some residues compared to the sequences of several flavivirus NS1 proteins. The virus with the closest identity percentage is the Ilhéus virus (74.5–73.37%), which is also considered a member of the same species [31]. This comparison made it possible to identify unique regions of the ROCV NS1 sequence that are not present in the sequences of the other analyzed viruses; these amino acid sequences were selected for the following analyses of peptide prediction.

2.2. Predicted Protein Characteristics and Structural Features of ROCV NS1

The full-length ROCV NS1 protein (353 aa, 40.06 kDa) was predicted to contain 61 basic, 50 acidic, 83 polar, and 130 nonpolar residues and 12 cysteine residues, and to have an isoelectric point of 6.93. The predicted charge density (Supplementary Figure S1A), disorder (Supplementary Figure S1B), flexibility (Supplementary Figure S1C), hydropathy (Supplementary Figure S2A–C), amphiphilicity (Supplementary Figure S2D), secondary structure (Supplementary Figure S3), stability (Supplementary Figure S4A–C), and surface probability (Supplementary Figure S4D) were obtained using DNASTAR Lasergene Protean

3D software, and are presented in the Supplementary Material. The Protean 3D algorithm uses these parameters simultaneously in antigen prediction, and these analyses were performed as a prerequisite for the antigenicity prediction analyses. The antigen prediction methods used are based on the physicochemical properties of amino acid residues and their abundance [32–34], performed by powerful software that compares these variables simultaneously.

2.3. Peptide Candidate as a Potential Antigen Suitable for Immunodiagnostic Tests

Analysis using the Jameson–Wolf (Figure 1A) and Welling methods (Figure 1B) found antigenic regions throughout nearly the entirety of the protein, with 23 main antigenic regions predicted by the former and 21 by the latter, respectively (Table 1). B-cell epitope prediction analysis using Protean 3D software revealed 48 highly antigenic regions (Figure 1C). These regions were selected and checked for their presence in the other NS1 flavivirus sequences through careful inspection of the alignment with that of other flaviviruses protein NS1 sequences previously retrieved from the VIPR server (Supplementary Excel file—see full description in “Sequence retrieval” in the Materials and Methods), and 3 antigenic regions were found to be present only in ROCV NS1: NS1^{91–108} (p_ROCV1), NS1^{121–131} (p_ROCV2), and NS1^{269–280} (p_ROCV3). Their antigenicity values were confirmed using the ElliPro server and the Bepipred Linear Epitope Prediction server, both of which predicted epitopes in the NS1^{121–131} peptide region. We therefore consider the p_ROCV2 peptide (SFLFKTQMANS) a promising target for developing a specific ROCV immunodiagnostic assay, as its region continues to be predicted in all these analyses, while the p_ROCV1 and p_ROCV3 peptides did not have their regions predicted concomitantly in these analyses. Therefore, the p_ROCV1 and p_ROCV3 peptides were discarded. As a final confirmation, we submitted the peptide sequence to the VaxiJen server, which yielded an antigenicity score of 0.5951 (threshold = 0.4). The peptide was also analyzed on the BLASTp online server (<https://blast.ncbi.nlm.nih.gov/Blast.cgi?PAGE=Proteins>, (accessed on 2 April 2022)), and no sequence overlap with any other flavivirus was identified, which is important to avoid possible cross-reactions with viruses of the same family.

Table 1. Epitope predictions for ROCV NS1 based on the immunotools.

Prediction Items	Prediction Results (Location of Deduced Peptides)
Antigenicity: Jameson–Wolf, DNASTAR Protean 3D	1–4, 11–17, 24–25, 28–42, 49–54, 59–62, 106–109, 118–119, 136–146, 171–177, 189–191, 203–209, 220–224, 235–241, 249–273, 279–289, 291–295, 302–309, 313, 316–318, 320, 324–328, 335–345
Antigenicity: Welling, DNASTAR Protean 3D	26, 30–40, 44–48, 51, 61–62, 66, 72–73, 89, 91, 94–104, 145, 168, 170–174, 191–197, 210, 213, 250–261, 264, 295–301, 303, 341–342, 349–353
B-cell epitopes: high antigenic regions, DNASTAR Protean 3D	2–5, 10, 12–14, 16, 21–23, 26, 34–36, 40–41, 48–51, 53, 71–76, 78, 80–83, 88–91, 99, 101–102, 111, 113–118, 124–127, 134–137, 140, 147, 149–150, 153–164, 169–171, 174, 176–185, 187–191, 193–199, 201–205, 215–216, 220–228, 232–241, 247–249, 252–253, 260–266, 270–271, 273–278, 280, 282–283, 302–305, 309–310, 312–313, 315–320, 328–330, 341–342, 352
ElliPro antibody epitope prediction (IEDB)	1–23, 47–55, 73–87, 104–132, 139–147, 205–210, 230–241, 279–297, 299–320, 337–351
Bepipred linear epitope prediction (IEDB)	25–41, 93–131, 137–150, 173–178, 228–240, 248–275, 281–282, 290–317, 319–319, 339–349
ABCpred prediction server	2–18, 16–32, 25–41, 50–66, 93–109, 107–123, 118–134, 124–140, 138–154, 159–175, 182–198, 193–209, 204–220, 219–235, 229–245, 248–264, 273–289, 306–322, 314–330, 329–345



Figure 1. Prediction of antigenicity and linear B-cell epitopes of ROCV NS1. (A) Antigenicity prediction using the Jameson–Wolf method. (B) Antigenicity prediction using the Welling method. (C) B-cell epitopes, high antigenic regions. The antigenic propensities of the antigens were greater than 1.0, indicating that this protein is highly antigenic.

2.4. Physicochemical Properties of the p_ROCV2 Peptide

The physicochemical properties of the p_ROCV2 peptide were predicted using the ProtParam tool (<http://web.expasy.org/protparam/>, (accessed on 5 April 2022)). According to this prediction analysis, the peptide is 1.27 kDa, has basic features (pI 8.47), and is probably non-hydrophobic, even though the index was low (GRAVY score: -0.009). Furthermore, p_ROCV2 may be stable under natural conditions (the instability score was 0.21). The yeast half-life time in vivo exceeded 20 hours.

2.5. Tri-Dimensional ROCV NS1 Hexamer Protein and Immunogenic Peptide Analyses

Structure analysis from the I-TASSER model output (NS1 monomer) obtained a clash-score (score of serious steric overlaps) of 4.68, placing this protein in the 95th percentile (100 = best, among structures of comparable resolution). The Ramachandran plot (Supplementary Figure S5) showed 20 outlier (ϕ/ψ angles) residues, with 94.3% of all residues in allowed regions. These results indicate the high quality of the protein modeled by the I-TASSER server. As described above, this structure was used to model the dimer and hexamer NS1 oligomer states; the structures are presented in Figure 2.

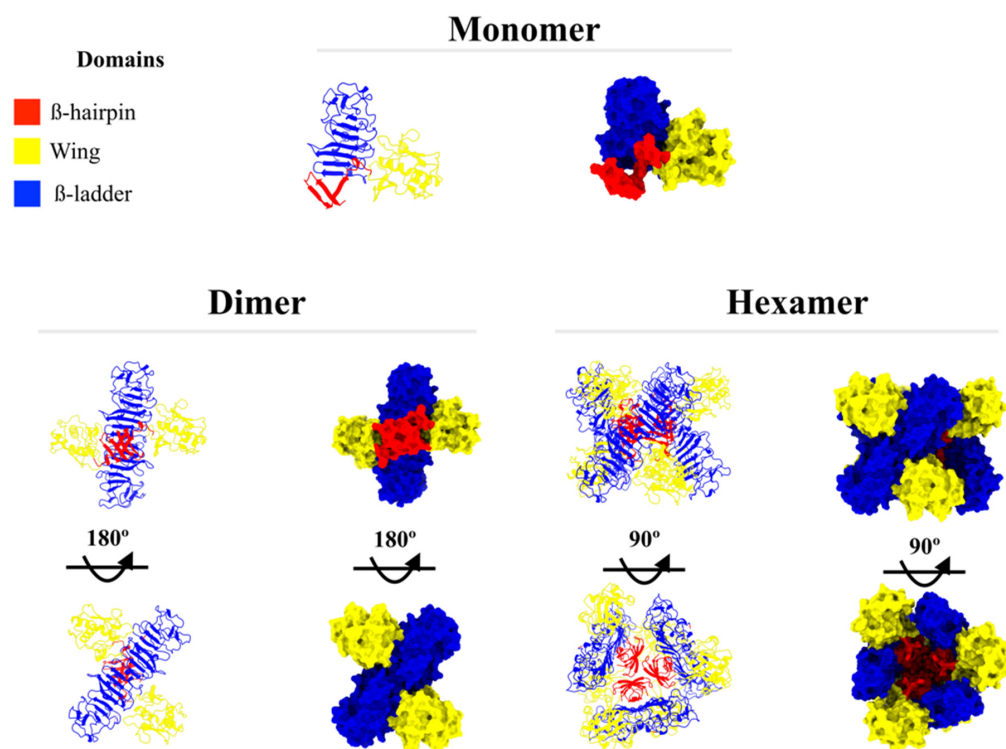


Figure 2. Different NS1 oligomeric states. In the figure, NS1 is represented as a monomer, dimer, and hexamer in both ribbon and surface and colored according to well-described domains: β -hairpin (residues 1–30) in red, wing (residues 31–180) in yellow, and β -ladder (residues 181–352) in blue.

The RMSD analysis found that the protein as a hexamer reached stability at around 50 ns of simulation (Figure 3A); the RMSD of initial structure and frame 5 ns ago as a reference stabilized at around 0.5 to 0.6 nm and 0.1 to 0.2 nm, respectively. These results show that the 200 ns of simulation was sufficient to obtain protein stability in solution.

The RMSF analysis (Figure 3B) shows the mean fluctuation by residue; note that the fluctuations are very similar among the six chains (different color lines). Higher fluctuations were observed in the wing domain, particularly between residues 116 to 143, where the potential immunogenic peptide (residues 121 to 131) is located. This domain may interact with the structural protein prM/E at times to assist in membrane bending [15], which could cause increased fluctuations when interaction is absent.

The cluster analysis was performed using two different cutoff values: 0.15 nm and 0.20 nm. Cluster analysis is primarily used to evaluate protein stability along with RMSD and radius of gyration. For this purpose, the most similar structures are grouped into conformational groups (clusters). Here we use the smallest value that results in fewer than 10 conformational clusters. We start with the definition of 0.15 nm and increase the value by 0.5 nm. If the smallest value is between 0.15 and 0.25 nm and there is a single conformational cluster along the trajectory, especially after RMSD stabilization, this indicates that this protein group is the most stable conformation.

The method for cluster determination (GROMOS) counts the number of neighbors using the cutoff, takes the structure with the largest number of neighbors with all its neighbors as the cluster, and eliminates it from the pool of clusters, then repeats the process for the remaining structures in the pool. The 0.15 nm cutoff found 36 clusters and did not show stability among the clusters (data not shown). Using the 0.20 nm cutoff, eight clusters were found (Figure 3C). Cluster #1, which was most present along the trajectory, appeared near 50 ns (when protein stability was reached, as observed in the RMSD analysis). The central structure (with the smallest average RMSD value of all other structures in the cluster) of cluster #1 was used for visual structure analysis.

Figure 3D shows the radius of gyration, which began around 4.11 nm and after 20 ns ranged from 4.10 to 4.05 nm. This small variation indicates that the protein structure did not change significantly throughout the MD simulation.

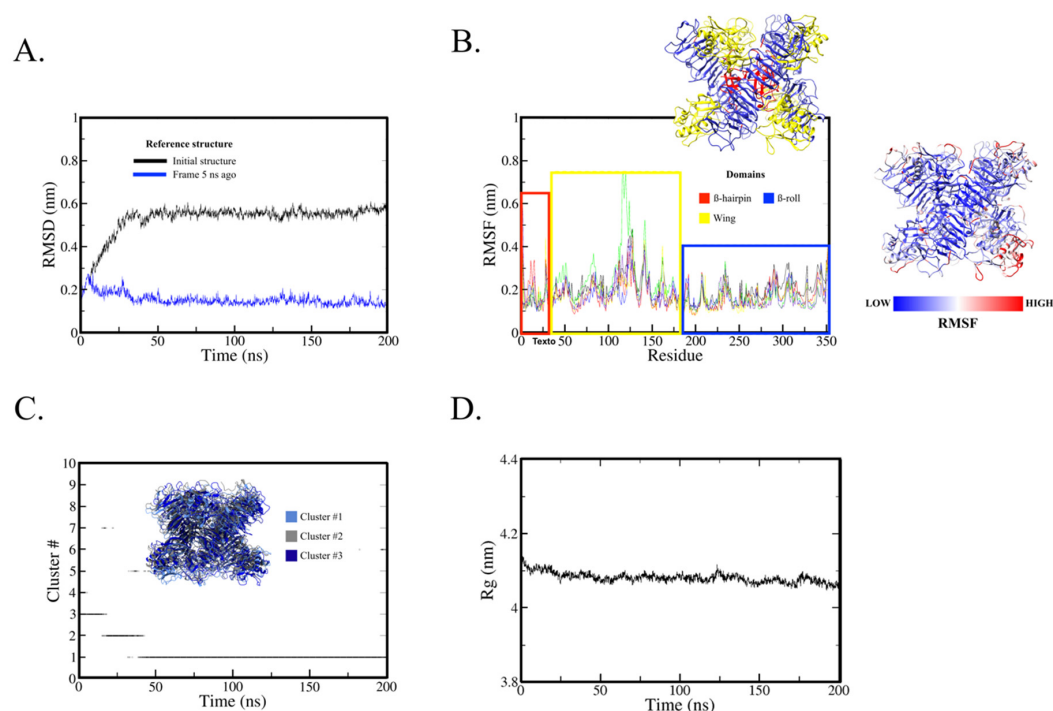


Figure 3. Molecular dynamics analysis of NS1 hexamer in solution. (A) RMSD trajectory analysis using the initial structure (black line) as reference structure and the previous 5 ns frame (blue line). (B) RMSF per residue and per chain. Each line color represents one chain of the hexamer. Because they are identical, the difference is not required or significant for the analysis here. The colored rectangles highlight NS1 domains: β -hairpin (residues 1–30) in red, wing (residues 31–180) in yellow, and β -ladder (residues 181–352) in blue; a ribbon representation is also included with the same color scheme. A second ribbon representation of the hexamer structure based on RMSF value is shown at right (blue indicating low and red high), demonstrating that this fluctuation occurs in the wing domain. (C) Cluster analysis using 0.2 nm for conformational grouping. Three main clusters were observed (represented in the ribbon) where cluster #1 emerges near 50 ns when RMSD stability is observed. (D) Radius of gyration plot showing low variation rate, suggesting the protein did not change structurally along the trajectory.

The solvent accessible surface area (SASA) of the immunogenic peptide (residues 121 to 131) was also calculated, with the graphic results for the average SASA value per NS1 chain (monomer) presented in Figure 4A; the average value remained around 190 to 195 nm². As seen in Figure 4B, average SASA decreased from 18 nm² to 16 nm² by the end of the simulation. This decrease was mainly caused by chain C (green line), which reached 14 nm². In this way, the average peptide SASA is approximately 8–10% of the protein SASA value. The individual SASA plot for each protein chain can be seen in Supplementary Figures S6 and S7.

Note that each NS1 hexamer has six of these epitopes (as seen in Figure 4), which are not close to each other. Since this protein is secreted and found in human plasma during infection, the chance of antibody recognition and binding could be increased. In fact, other studies have described antibodies targeting the wing domain in other flavivirus species [35,36], and a wing domain peptide has been suggested as a potential target for a dengue vaccine candidate [37].

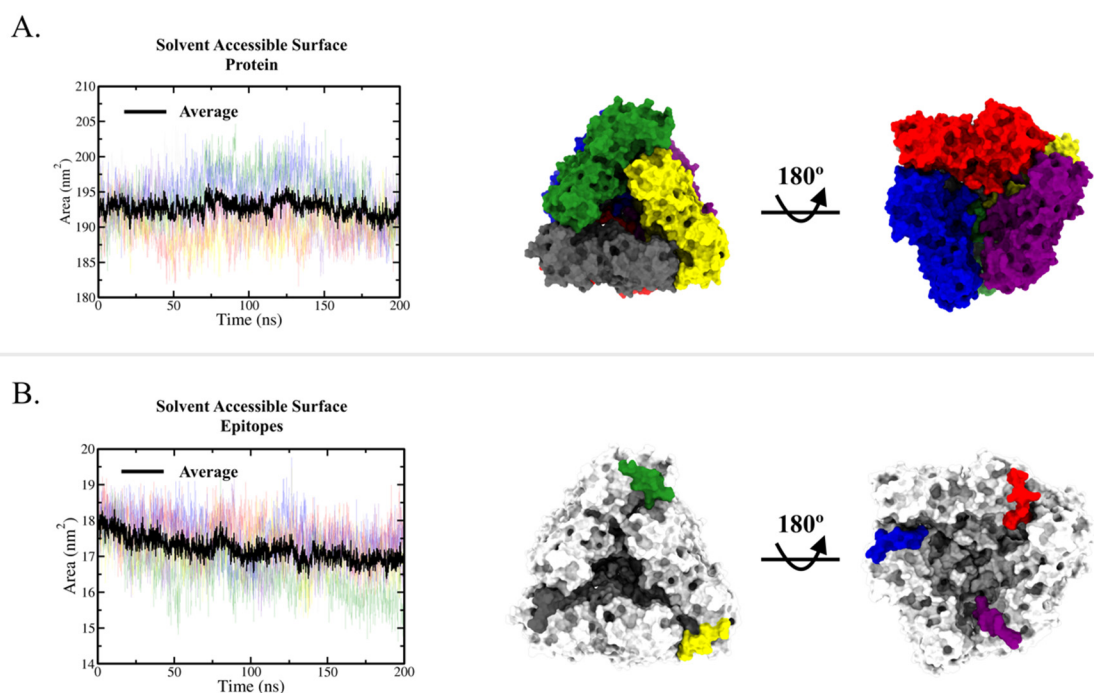


Figure 4. Solvent accessible surface analysis. (A) Solvent accessible surface plot of the entire protein per chain (transparent colored lines), with the average presented as the black line. Two surface representations are shown at right, colored by the individual chain. (B) Solvent accessible surface plot of peptide (residues 121 to 131) in transparent colored lines, with the average presented as the black line. Two surface representations are shown at right; the protein is in white and peptides (residues 121–131) are colored as the chains in panel (A). Individual SASA plots for protein and peptide are presented in Supplementary Figures S6 and S7.

3. Discussion

Studies have confirmed ROCV circulates in urban [3,38] and rural environments [7,39], and most infections by the virus are assumed to be asymptomatic or associated with nonspecific symptoms [3]. For these reasons, seroprevalence surveys offer a potential method for assessing the true prevalence of ROCV (since this value is currently unknown due to the lack of national surveys). In this scenario, identifying linear B-cell epitopes could offer an approach to improve and accelerate the development of novel diagnostic tests to effectively determine the seroprevalence of ROCV.

This study identified B-cell epitopes in antigen candidates for developing serological tests for ROCV. We explored ROCV NS1, a protein highlighted as a very strong immun-

odominant marker for both acute and persistent forms of flavivirus fever [40], a strongly immunogenic protein [41] considered a reliable serodiagnosis marker of infection by other flaviviruses [42,43]. Our antigenicity predictions using different methodologies indicated the probable high immunogenicity and antigenicity of ROCV NS1, but the use of whole antigens in serodiagnosis may result in cross-reactivity with other related flaviviruses, and for this reason B-cell epitope identification is a promising alternative to improve the specificity of serological tests for ROCV.

In recent years, combinations of prediction algorithms have been used to improve the accuracy of linear B-cell epitope predictions against viruses [44–47], fungi [48], protozoa [49,50], and bacteria [51–54]. However, no *in silico* study has predicted linear B-cell epitopes of ROCV, only for other flaviviruses, and the targeting focused on the envelope protein [55–60], prM [57,60], NS1 [18,60–62], NS3, and NS5 [62], with similar algorithms used individually to explore the targets, predicting linear B-cell epitopes in each protein studied.

If we consider only studies with the NS1 protein, a monoclonal antibody (mAb) against DENV (2B7) has been described to affect the NS1 wing domain, which is thought to be critical for NS1 binding to cells [63]. Studies with mAbs against WNV were inconclusive regarding specific recognition of NS1 amino acids, but mAbs were thought to bind to residues 1–157, which form part of the wing domain [64]. Against ZIKV, mAbs binding to the wing domain (residues 146–Z15 mAb; residues 101 and 177–178–ZIKV-292 mAb) were found to be protective in pregnant and non-pregnant mice [65]. Two mAbs (2H5 and 4H1BC) were found to bind to wind residues 193–209 of ZIKV and DENV2, which is related to cross-reactivity and not suitable for a specific diagnostic test [63].

In this study, many sequences were predicted as epitopes by a combination of algorithms (B-cell epitope high antigenic regions from DNASTAR Protean 3D, Bepipred, ElliPro, and ABCpred), offering a choice of many potential peptides, and the deciding factor was the absence of the peptide in other flaviviruses. After combining this initial epitope identification with the antigenic analysis, we predicted only one epitope. Notably, even though all the predicted epitopes were conserved in the ROCV strains described in the ViPR database, the lack of studies on ROCV polymorphism hampers conclusions about the actual conservation of the identified epitopes in ROCV strains, because of the significant difficulty involved in identifying new cases and isolating the virus. In a review study of NS1 epitopes of different flaviviruses, no epitope regions encompassing residues 121–131 of NS1 were found [40]. This may indicate that the described epitope in this study has high potential to not cross-react with other flaviviruses. However, further studies should be performed to ensure this specificity.

A previous study hypothesized that predicted epitopes which fail during experimental validation could be buried in protein quaternary structures [47], thus impeding prediction algorithms. Considering this hypothesis as well as the oligomerization of similar proteins [66,67], we evaluated the locations of predicted epitopes in the oligomeric structures of the investigated proteins. We modeled the quaternary structures of these proteins and observed that the p_ROCV2 peptide was exposed in the NS1 hexamer (Figure 4). From our perspective, similar assessments of the presence of predicted epitopes in the oligomeric structure of the protein may be essential to improve the accuracy of epitope prediction, and the lack of such analyses could at least partly explain the low validation rates of predicted epitopes for some infectious agents seen in other studies with similar methodologies.

In Brazil, although the presence of ROCV has been demonstrated in animals [6,39] and humans [3], ROCV infections remain poorly understood and reported. Moreover, even though ROCV infection could be mistaken for dengue [3,8] or other infectious diseases, no cases are investigated as ROCV infection in Brazil, which corroborates the under-reporting of this zoonosis and explains the limited number of ROCV samples, which in turn may be a limiting factor for immunoassay validation tests.

4. Materials and Methods

4.1. Sequence Retrieval

The full amino acid sequences of several medically relevant flavivirus NS1 proteins isolated from different endemic countries were retrieved from the Virus Pathogens Research (ViPR) database (<https://www.viprbrc.org>, (accessed on 3 March 2022)) (see Supplementary Excel file) and aligned using Mega 7.0 software (Mega, Raynham, MA, USA). The alignment showed that the protein sequences of ROCV strains are preserved; although the other flaviviruses used for comparison are in the same genus, their complete amino acid sequences for the NS1 protein differ from the ROCV sequence, with different identity percentages (see Supplementary Table S1). Representative sequences of ROCV (GenBank Access 009553341, ATG32103, and AAV34158) were selected for antigenicity analyses and molecular dynamics (MD) simulations.

4.2. Predicting Physicochemical Properties of Protein

To better understand the biophysical characteristics of the protein, prediction analyses were performed using DNASTAR Lasergene software (DNASTAR Inc., Madison, WI, USA): amphiphilicity according to the Eisenberg method (predicts amphiphilic regions by identifying periodic changes in hydrophobicity, where period length can suggest the underlying secondary structure), charge density according to the Lehninger method (predicts charged regions for a given pH by identifying ranges with an increased positive or negative character), and disorder according to the JRONN method (predicts structurally disordered regions by using an artificial neural network algorithm to identify sequence patterns suggestive of a disordered region). The secondary structure was predicted by the Chou–Fasman method (predicts the location of secondary structure elements using a rule-based method involving the propensities of amino acids occurring in helix, sheet, and turn conformations), the Deléage–Roux method (predicts the location of secondary structure elements using a classification method based on the propensities of amino acids occurring in helix, sheet, turn, and coil conformations), the Garnier–Robson method (predicts the location of secondary structure elements using statistical methods: when GOR I and GOR II are based on the propensities of amino acids occurring in helix, sheet, turn, and coil conformations and GOR IV is based on residue pair frequencies occurring in helix, sheet, and coil conformations), and the coiled coil method (predicts the location of coiled coils using a statistical method that estimates the probability of observing a sequence in a coiled coil compared to that in a globular structure). Stability was verified according to the aliphatic index, instability index, and isoelectric precipitate.

4.3. Predicting Antigenicity and Linear B-Cell Epitopes

After interacting with antigens (such as B-cell epitopes), B-lymphocyte cells differentiate into memory cells and antibody secreting plasma cells [68]. B-cell epitopes are hydrophilic and accessible for flexible regions [69]. DNASTAR Lasergene software was used to obtain hydrophathy prediction values according to the Hopp–Woods [70], Kyte–Doolittle [71], and Parker methods [72], along with Emini prediction values of surface accessibility [73] and Karplus and Schulz flexibility prediction values [74]. The results were confirmed via online analysis in the IEDB server (<http://www.iedb.org/>, (accessed on 2 April 2022)). B-cell epitopes were also predicted using DNASTAR Lasergene software (DNASTAR Inc., Madison, WI, USA) [75], with a machine learning approach to identify patterns in secondary structure, flexibility, hydrophathy, and antigenicity suggestive of an epitope (threshold = 0.5), and subsequently confirmed using the ElliPro server (<http://tools.iedb.org/ellipro/>, (accessed on 2 April 2022)), ABCpred (https://webs.iitd.edu.in/raghava/abcpred/ABC_submission.html, (accessed on 2 April 2022)), and the Kolaskar and Tongaonkar antigenicity scale (<http://tools.immuneepitope.org/bcell/>, (accessed on 2 April 2022)). ElliPro utilizes the protrusion index (PI) of residues, protein shape approximation, and the final neighboring residue clustering, which relies on PI [76]. The Kolaskar and Tongaonkar antigenicity scale is a semiempirical epitope prediction method with

more than 75% prediction accuracy [32]. Antigenicity was analyzed using the Jameson–Wolf method [33] (which predicts immunogenic regions by identifying ranges with an increased antigenic index derived from predictions of hydrophilicity, surface accessibility, flexibility, and turn or coil conformations) and the Welling method [34] (which predicts immunogenic regions by identifying ranges with an increased antigenic profile based on the propensities of amino acids in known antigenic sites). Regions of amino acid sequences unique to the ROCV NS1 protein that were predicted as probable antigens were submitted to a second online antigenicity prediction platform, VaxiJen (<http://www.ddg-pharmfac.net/vaxijen>, (accessed on 2 April 2022)) [77], an alignment-independent antigen predictor with 87% viral epitope prediction accuracy [78].

4.4. Predicting Physicochemical Properties of the Epitopes

Physicochemical properties of the ROCV antigenic sequences including half-life, instability index, aliphatic index, theoretical pI, and hydrophaticity value were predicted using the ProtParam online tool (<http://web.expasy.org/protparam/>, (accessed on 4 April 2022)) [79]. The half-life prediction estimates how long a peptide remains stable in prokaryotic and eukaryotic organisms. A protein is considered stable when the value obtained is lower than the cutoff value of 40, while the hydrophaticity index evaluates the probability that a region is hydrophobic (positive values) or hydrophilic (negative values). A graphic representation generated by the MD simulation was used to assess the secondary structure of the peptide.

4.5. NS1 Hexamer Modeling

The NS1 protein as a monomer from ROCV was modeled using the I-TASSER server [80]. The input sequence in FASTA format was retrieved from the SPH 34,675 strain (GenBank Access 009553341, ATG32103, and AAV34158). The output model was then analyzed via MolProbity to evaluate structure protein quality.

After the structure was validated, the protein coordinates were submitted to the GRAMM-X server [81] to obtain the dimeric NS1 structure. The ten resulting models were evaluated, and the structure that matched the crystallographic dimeric NS1 deposited in the Protein Data Bank (PDB) was selected for hexamer modeling.

Finally, the hexamer structure of NS1 was modeled using the same server after the dimer structure was obtained. The output file was a hexamer protein resulting from three dimer oligomerization. Unlike the NS1 dimer, no crystallographic NS1 hexamer is available in PDB: the selected output structure was based on previous studies describing the NS1 hexamer structure [82].

4.6. Molecular Dynamics Simulation

After modeling, the structure was prepared for MD simulation using the PropKa server [83] for histidine protonation prediction at physiological pH (7.4). The protein underwent MD simulation with GROMACS 2021.2 software [84] and the AMBER99SB-ILDN force field. A cubic box was created around the protein structure with a minimum distance of 1.2 nm between any protein atom and the box edge. The TIP3P water model was added to the box, and the system was neutralized with six sodium (Na^+) ions.

To constrain all bonds except the water bonds, the LINCS algorithm [85] was applied, and the SETTLE algorithm [86] was applied for the water bonds. In the equilibration step, system temperature and pressure were adjusted to 310 K and 1 atm, respectively. The temperature was regulated using the modified Berendsen [87] algorithm (also known as the V-rescale algorithm), and pressure was regulated according to Parrinello–Rahman [88]. The Particle Mesh Ewald summation method was used to calculate long-range electrostatic interaction, and for non-bonded interactions a 1.0 nm cutoff was defined. The leap-frog algorithm [89] was applied using a 2 fs time step to integrate motion equations.

The system was then subjected to a two-step energy minimization. The first step was set to perform in 500 steps or when the maximum force reached a value below

50 kJ/mol/nm using the steepest descent algorithm with protein position constraint. The second step used the same algorithm and flexible water without protein restraint. Additionally, the number of steps was increased for 10,000 steps or when the maximum force reached a value below 250 kJ/mol/nm.

In this way, after the minimization steps, the system was equilibrated using the parameters and algorithms described above. This equilibration step was comprised of two 100 ps simulations: NVT ensemble (constant number of particles, volume, and temperature) and NPT ensemble (constant number of particles, pressure, and temperature) for thermodynamics equilibration with protein position constraint. Finally, before the production run, an additional equilibration was performed with an NPT ensemble of 1 ns without protein position constraint. The MD production run was carried out at 310 K and 200 ns without protein conformation constraint in the NPT ensemble.

Trajectory analysis was conducted using a root mean square deviation (RMSD) calculation using the first frame and the previous 5 ns frame as a reference structure to evaluate protein stability. Root mean square fluctuation (RMSF) analysis evaluating the average fluctuation per residue of the entire trajectory was also performed. Radius of gyration (Rg) is a metric related to the compactness of a protein and was also calculated here. Finally, the *g_cluster* package in GROMACS software using the GROMOS algorithm as described by Daura et al. [90], UCSF Chimera visualization software [91], and UCSF ChimeraX [92] were used to analyze the protein structure and render images. This MD protocol was successfully utilized previously to predict peptide antigens in the Mayaro virus [93].

5. Conclusions

The antigenic sequence identified in ROCV NS1 offers potential for developing immunodiagnostic platforms. We suggest constructing a structural model of the ROCV NS1 hexamer to better understand its structure and behavior, and also as a base for further studies involving mutagenesis and drug therapy against ROCV, a flavivirus that causes encephalitis. Finally, the results obtained from this study will be applied in subsequent confirmatory in vitro testing.

Supplementary Materials: The following supporting information can be downloaded at: <https://www.mdpi.com/article/10.3390/ijms23147681/s1>.

Author Contributions: Conceptualization, M.V.S., V.G.d.C. and G.d.L.M.; methodology, M.V.S., V.G.d.C., G.d.L.M. and R.A.D.S.; validation, M.V.S., G.d.L.M. and R.A.D.S.; formal analysis, R.A.D.S.; resources, G.C.D.d.S. and M.L.N.; visualization, R.E.M.; writing—original draft preparation, M.V.S. and G.d.L.M.; supervision, R.A.D.S. and M.L.N.; funding acquisition, G.C.D.d.S. and M.L.N. All authors have read and agreed to the published version of the manuscript.

Funding: This research was funded by grant 2013/21719-3 from FAPESP (Fundação de Amparo à Pesquisa do Estado de São Paulo). M.L.N. is partially supported by the Centers for Research in Emerging Infectious Disease via The Coordinating Research on Emerging Arboviral Threats Encompassing the Neotropics (CREATE-NEO) grant U01AI151807 awarded by the National Institutes of Health (NIH/USA). M.L.N. is a CNPq Research Fellow. M.V.S. was supported by a FAPESP PhD Scholarship, process 2020/12875-5. G.d.L.M. was supported by a CAPES PhD Scholarship, process 88887.659079/2021-00.

Institutional Review Board Statement: Not applicable.

Informed Consent Statement: Not applicable.

Data Availability Statement: Not applicable.

Acknowledgments: The authors wish to thank LaMCAD (the Multiuser High-Performance Computing Laboratory) at the Universidade Federal de Goiás for allowing them to use their high-performance cluster.

Conflicts of Interest: The authors declare no conflict of interest.

References

1. Tiriba, A.C.; Miziara, A.M.; Lorenço, R.; Costa, C.R.B.; Costa, C.S.; Pinto, G.H. Encefalite Humana Primária Epidêmica Por Arbovírus Observada No Litoral Sul Do Estado de São Paulo. *Rev. Assoc. Med. Brasil* **1976**, *22*, 415–420.
2. Saivish, M.V.; Gomes da Costa, V.; de Lima Menezes, G.; Alves da Silva, R.; Dutra da Silva, G.C.; Moreli, M.L.; Sacchetto, L.; Pacca, C.C.; Vasilakis, N.; Nogueira, M.L. Rocio Virus: An Updated View on an Elusive Flavivirus. *Viruses* **2021**, *13*, 2293. [[CrossRef](#)]
3. Saivish, M.V.; da Costa, V.G.; Rodrigues, R.L.; Féres, V.C.R.; Montoya-Diaz, E.; Moreli, M.L. Detection of Rocio Virus SPH 34675 during Dengue Epidemics, Brazil, 2011–2013. *Emerg. Infect. Dis.* **2020**, *26*, 797–799. [[CrossRef](#)]
4. Lopes, O.D.S.; Coimbra, T.L.M.; Sacchetta, L.D.A.; Calisher, C.H. Emergence of a new arbovirus disease in Brazil: I. isolation and characterization of the etiologic agent, Rocio virus. *Am. J. Epidemiol.* **1978**, *107*, 444–449. [[CrossRef](#)]
5. Iversson, L.B. Aspectos da epidemia de encefalite por arbovirus na região do Vale do Ribeira, S. Paulo, Brasil, no período de 1975 a 1978. *Rev. Saúde Pública* **1980**, *14*, 9–35. [[CrossRef](#)]
6. Pauvolid-Corrêa, A.; Campos, Z.; Juliano, R.; Velez, J.; Nogueira, R.M.R.; Komar, N. Serological Evidence of Widespread Circulation of West Nile Virus and Other Flaviviruses in Equines of the Pantanal, Brazil. *PLoS Negl. Trop. Dis.* **2014**, *8*, e2706. [[CrossRef](#)]
7. Silva, J.R.; Romeiro, M.F.; de Souza, W.M.; Munhoz, T.D.; Borges, G.P.; Soares, O.A.B.; de Campos, C.H.C.; Machado, R.Z.; Silva, M.L.C.R.; Faria, J.L.M.; et al. A Saint Louis Encephalitis and Rocio Virus Serosurvey in Brazilian Horses. *Rev. Soc. Bras. Med. Trop.* **2014**, *47*, 414–417. [[CrossRef](#)]
8. Straatmann, A.; Santos-Torres, S.; Vasconcelos, P.F.C.; Travassos da Rosa, A.P.A.; Rodrigues, S.G.; Tavares-Neto, J. Evidências sorológicas da circulação do arbovírus Rocio (Flaviviridae) na Bahia. *Rev. Soc. Bras. Med. Trop.* **1997**, *30*, 511–515. [[CrossRef](#)]
9. Tanaka, H.; Weigl, D.R.; de Souza Lopes, O. The Replication of Rocio Virus in Brain Tissue of Suckling Mice. Study by Electron Microscopy. *Arch. Virol.* **1983**, *78*, 309–314. [[CrossRef](#)]
10. Setoh, Y.X.; Amarilla, A.A.; Peng, N.Y.; Slonchak, A.; Periasamy, P.; Figueiredo, L.T.M.; Aquino, V.H.; Khromykh, A.A. Full Genome Sequence of Rocio Virus Reveal Substantial Variations from the Prototype Rocio Virus SPH 34675 Sequence. *Arch. Virol.* **2018**, *163*, 255–258. [[CrossRef](#)]
11. Tsai, C.-L.; Sun, D.-S.; Su, M.-T.; Lien, T.-S.; Chen, Y.-H.; Lin, C.-Y.; Huang, C.-H.; King, C.-C.; Li, C.-R.; Chen, T.-H.; et al. Suppressed Humoral Immunity Is Associated with Dengue Nonstructural Protein NS1-Elicited Anti-Death Receptor Antibody Fractions in Mice. *Sci. Rep.* **2020**, *10*, 6294. [[CrossRef](#)] [[PubMed](#)]
12. Shukla, A.; Rastogi, M.; Singh, S.K. Zika Virus NS1 Suppresses the Innate Immune Responses via MiR-146a in Human Microglial Cells. *Int. J. Biol. Macromol.* **2021**, *193*, 2290–2296. [[CrossRef](#)] [[PubMed](#)]
13. Avirutnan, P.; Hauhart, R.E.; Somnuk, P.; Blom, A.M.; Diamond, M.S.; Atkinson, J.P. Binding of Flavivirus Nonstructural Protein NS1 to C4b Binding Protein Modulates Complement Activation. *J. Immunol.* **2011**, *187*, 424–433. [[CrossRef](#)]
14. Ci, Y.; Liu, Z.-Y.; Zhang, N.-N.; Niu, Y.; Yang, Y.; Xu, C.; Yang, W.; Qin, C.-F.; Shi, L. Zika NS1-Induced ER Remodeling Is Essential for Viral Replication. *J. Cell Biol.* **2020**, *219*, e201903062. [[CrossRef](#)] [[PubMed](#)]
15. Scaturro, P.; Cortese, M.; Chatel-Chaix, L.; Fischl, W.; Bartenschlager, R. Dengue Virus Non-Structural Protein 1 Modulates Infectious Particle Production via Interaction with the Structural Proteins. *PLoS Pathog.* **2015**, *11*, e1005277. [[CrossRef](#)]
16. Roldán, J.S.; Cassola, A.; Castillo, D.S. Development of a Novel NS1 Competitive Enzyme-Linked Immunosorbent Assay for the Early Detection of Zika Virus Infection. *PLoS ONE* **2021**, *16*, e0256220. [[CrossRef](#)]
17. Lorch, M.S.; Collado, M.S.; Argüelles, M.H.; Rota, R.P.; Spinsanti, L.I.; Lozano, M.E.; Goñi, S.E. Production of Recombinant NS1 Protein and Its Possible Use in Encephalitic Flavivirus Differential Diagnosis. *Protein Expr. Purif.* **2019**, *153*, 18–25. [[CrossRef](#)] [[PubMed](#)]
18. Lee, H.-J.; Cho, Y.; Kang, H.J.; Choi, H.; Han, K.R.; Chong, C.K.; Kim, Y.B. Identification of Peptide Based B-Cell Epitopes in Zika Virus NS1. *Biochem. Biophys. Res. Commun.* **2018**, *505*, 1010–1014. [[CrossRef](#)]
19. Kumarasamy, V.; Wahab, A.H.A.; Chua, S.K.; Hassan, Z.; Chem, Y.K.; Mohamad, M.; Chua, K.B. Evaluation of a Commercial Dengue NS1 Antigen-Capture ELISA for Laboratory Diagnosis of Acute Dengue Virus Infection. *J. Virol. Methods* **2007**, *140*, 75–79. [[CrossRef](#)]
20. Zainah, S.; Wahab, A.H.A.; Mariam, M.; Fauziah, M.K.; Khairul, A.H.; Roslina, I.; Sairulakhma, A.; Kadimon, S.S.; Jais, M.S.M.; Chua, K.B. Performance of a Commercial Rapid Dengue NS1 Antigen Immunochromatography Test with Reference to Dengue NS1 Antigen-Capture ELISA. *J. Virol. Methods* **2009**, *155*, 157–160. [[CrossRef](#)]
21. Castro-Jorge, L.A.; Machado, P.R.L.; Fávero, C.A.; Borges, M.C.; Passos, L.M.R.; de Oliveira, R.M.; Fonseca, B.A.L. Clinical Evaluation of the NS1 Antigen-Capture ELISA for Early Diagnosis of Dengue Virus Infection in Brazil. *J. Med. Virol.* **2010**, *82*, 1400–1405. [[CrossRef](#)] [[PubMed](#)]
22. Murphy, N.; Macchiaverna, N.P.; Victoria Cardinal, M.; Bhattacharyya, T.; Mertens, P.; Zeippen, N.; Gustin, Y.; Gilman, Q.; Gürtler, R.E.; Miles, M.A. Lineage-Specific Rapid Diagnostic Tests Can Resolve Trypanosoma Cruzi TcII/V/VI Ecological and Epidemiological Associations in the Argentine Chaco. *Parasit. Vectors* **2019**, *12*, 424. [[CrossRef](#)] [[PubMed](#)]
23. Kumar, M.; Malik, S.S.; Vergis, J.; Ramanjeneya, S.; Sahu, R.; Pathak, R.; Yadav, J.P.; Dhaka, P.; Barbuddhe, S.B.; Rawool, D.B. Development of the Com1 Synthetic Peptide-Based Latex Agglutination Test (LAT) and Its Comparative Evaluation with Commercial Indirect-ELISA for Sero-Screening of Coxiellosis in Cattle. *J. Microbiol. Methods* **2019**, *162*, 83–85. [[CrossRef](#)] [[PubMed](#)]

24. Guevarra, L.A., Jr.; Boado, K.J.O.; Ceñidoza, F.B.B.; Imbao, M.R.L.M.; Sia, M.J.G.; Dalmacio, L.M.M. A Synthetic Peptide Analog of in Silico-Predicted Immunogenic Epitope Unique to Dengue Virus Serotype 2 NS1 Antigen Specifically Binds Immunoglobulin G Antibodies Raised in Rabbits. *Microbiol. Immunol.* **2020**, *64*, 153–161. [[CrossRef](#)]
25. Köhler, H.; Liebler-Tenorio, E.; Hughes, V.; Stevenson, K.; Bakker, D.; Willemssen, P.; Bay, S.; Ganneau, C.; Biet, F.; Vordermeier, H.M. Interferon- γ Response of Mycobacterium Avium Subsp. Paratuberculosis Infected Goats to Recombinant and Synthetic Mycobacterial Antigens. *Front. Vet. Sci.* **2021**, *8*, 645251. [[CrossRef](#)]
26. Middleton, S.; Steinbach, S.; Coad, M.; McGill, K.; Brady, C.; Duignan, A.; Wiseman, J.; Gormley, E.; Jones, G.J.; Vordermeier, H.M. A Molecularly Defined Skin Test Reagent for the Diagnosis of Bovine Tuberculosis Compatible with Vaccination against Johne's Disease. *Sci. Rep.* **2021**, *11*, 2929. [[CrossRef](#)]
27. Polvere, I.; Parrella, A.; Casamassa, G.; D'Andrea, S.; Tizzano, A.; Cardinale, G.; Voccola, S.; Porcaro, P.; Stilo, R.; Vito, P.; et al. Seroprevalence of Anti-SARS-CoV-2 IgG and IgM among Adults over 65 Years Old in the South of Italy. *Diagnostics* **2021**, *11*, 483. [[CrossRef](#)]
28. Arumugam, S.; Nayak, S.; Williams, T.; di Santa Maria, F.S.; Guedes, M.S.; Chaves, R.C.; Linder, V.; Marques, A.R.; Horn, E.J.; Wong, S.J.; et al. A Multiplexed Serologic Test for Diagnosis of Lyme Disease for Point-of-Care Use. *J. Clin. Microbiol.* **2019**, *57*, e01142-19. [[CrossRef](#)]
29. Prado, I.C.; Mendes, V.G.; Souza, A.L.A.; Dutra, R.F.; De-Simone, S.G. Electrochemical Immunosensor for Differential Diagnostic of Wuchereria Bancrofti Using a Synthetic Peptide. *Biosens. Bioelectron.* **2018**, *113*, 9–15. [[CrossRef](#)]
30. Gomara, M.J.; Haro, I. Synthetic Peptides for the Immunodiagnosis of Human Diseases. *Curr. Med. Chem.* **2007**, *14*, 531–546. [[CrossRef](#)]
31. Genus: Flavivirus-Flaviviridae-Positive-Sense RNA Viruses-ICTV. Available online: https://talk.ictvonline.org/ictv-reports/ictv_online_report/positive-sense-rna-viruses/w/flaviviridae/360/genus-flavivirus (accessed on 16 May 2022).
32. Kolaskar, A.S.; Tongaonkar, P.C. A Semi-Empirical Method for Prediction of Antigenic Determinants on Protein Antigens. *FEBS Lett.* **1990**, *276*, 172–174. [[CrossRef](#)]
33. Jameson, B.A.; Wolf, H. The Antigenic Index: A Novel Algorithm for Predicting Antigenic Determinants. *Bioinformatics* **1988**, *4*, 181–186. [[CrossRef](#)] [[PubMed](#)]
34. Prediction of Sequential Antigenic Regions in Proteins-Welling-1985-FEBS Letters-Wiley Online Library. Available online: <https://febs.onlinelibrary.wiley.com/doi/abs/10.1016/0014-5793%2885%2980374-4?sid=nlm%3Apubmed> (accessed on 25 May 2022).
35. Wessel, A.W.; Doyle, M.P.; Engdahl, T.B.; Rodriguez, J.; Crowe, J.E.; Diamond, M.S. Human Monoclonal Antibodies against NS1 Protein Protect against Lethal West Nile Virus Infection. *mBio* **2021**, *12*, e02440-21. [[CrossRef](#)] [[PubMed](#)]
36. Modhiran, N.; Song, H.; Liu, L.; Bletchly, C.; Brillault, L.; Amarilla, A.A.; Xu, X.; Qi, J.; Chai, Y.; Cheung, S.T.M.; et al. A Broadly Protective Antibody That Targets the Flavivirus NS1 Protein. *Science* **2021**, *371*, 190–194. [[CrossRef](#)]
37. Lai, Y.-C.; Chuang, Y.-C.; Liu, C.-C.; Ho, T.-S.; Lin, Y.-S.; Anderson, R.; Yeh, T.-M. Antibodies Against Modified NS1 Wing Domain Peptide Protect Against Dengue Virus Infection. *Sci. Rep.* **2017**, *7*, 6975. [[CrossRef](#)]
38. Lopes, O.D.S.; Sacchetta, L.D.A.; Coimbra, T.L.M.; Pinto, G.H.; Glasser, C.M. Emergence of a new arbovirus disease in Brazil: II. epidemiologic studies on 1975 epidemic. *Am. J. Epidemiol.* **1978**, *108*, 394–401. [[CrossRef](#)]
39. Casseb, A.R.; Cruz, A.V.; Jesus, I.S.; Chiang, J.O.; Martins, L.C.; Silva, S.P.; Henriques, D.F.; Casseb, L.M.; Vasconcelos, P.F.C. Seroprevalence of Flaviviruses Antibodies in Water Buffaloes (Bubalus Bubalis) in Brazilian Amazon. *J. Venom. Anim. Toxins Trop. Dis.* **2014**, *20*, 9. [[CrossRef](#)]
40. Carpio, K.L.; Barrett, A.D.T. Flavivirus NS1 and Its Potential in Vaccine Development. *Vaccines* **2021**, *9*, 622. [[CrossRef](#)]
41. Rastogi, M.; Sharma, N.; Singh, S.K. Flavivirus NS1: A Multifaceted Enigmatic Viral Protein. *Virol. J.* **2016**, *13*, 131. [[CrossRef](#)]
42. Kam, Y.-W.; Leite, J.A.; Amrun, S.N.; Lum, F.-M.; Yee, W.-X.; Bakar, F.A.; Eng, K.E.; Lye, D.C.; Leo, Y.-S.; Chong, C.-Y.; et al. ZIKV-Specific NS1 Epitopes as Serological Markers of Acute Zika Virus Infection. *J. Infect. Dis.* **2019**, *220*, 203–212. [[CrossRef](#)]
43. Mora-Cárdenas, E.; Aloise, C.; Faoro, V.; Gašper, N.K.; Korva, M.; Caracciolo, I.; D'Agaro, P.; Avšič-Županc, T.; Marcello, A. Comparative Specificity and Sensitivity of NS1-Based Serological Assays for the Detection of Flavivirus Immune Response. *PLoS Negl. Trop. Dis.* **2020**, *14*, e0008039. [[CrossRef](#)] [[PubMed](#)]
44. Salarpour, A.; Toroghi, R.; Nikbakht Brujeni, G.; Momayez, R. In Silico Prediction of Linear B-Cell Epitopes for S1 Protein of Two Iranian 793/B Isolates and Their Changes after 90 Serial Passaging. *Vet. Res. Forum* **2020**, *11*, 365–370. [[CrossRef](#)] [[PubMed](#)]
45. Moeini, H.; Afridi, S.Q.; Donakonda, S.; Knolle, P.A.; Protzer, U.; Hoffmann, D. Linear B-Cell Epitopes in Human Norovirus GII.4 Capsid Protein Elicit Blockade Antibodies. *Vaccines* **2021**, *9*, 52. [[CrossRef](#)] [[PubMed](#)]
46. Sianez-Estrada, L.I.; Rivera-Benitez, J.F.; Rosas-Murrieta, N.H.; Reyes-Leyva, J.; Santos-López, G.; Herrera-Camacho, I. Immunoinformatics Approach for Predicting Epitopes in HN and F Proteins of Porcine Rubulavirus. *PLoS ONE* **2020**, *15*, e0239785. [[CrossRef](#)]
47. de Paiva Conte, F.; Tinoco, B.C.; Chaves, T.S.; de Oliveira, R.C.; Mansur, J.F.; Mohana-Borges, R.; de Lemos, E.R.S.; da Costa Neves, P.C.; Rodrigues-da-Silva, R.N. Identification and Validation of Specific B-Cell Epitopes of Hantaviruses Associated to Hemorrhagic Fever and Renal Syndrome. *PLoS Negl. Trop. Dis.* **2019**, *13*, e0007915. [[CrossRef](#)]
48. Almeida, M.A.; Almeida-Paes, R.; Guimarães, A.J.; Valente, R.H.; de Almeida Soares, C.M.; Zancopé-Oliveira, R.M. Immunoproteomics Reveals Pathogen's Antigens Involved in Homo Sapiens–Histoplasma Capsulatum Interaction and Specific Linear B-Cell Epitopes in Histoplasmosis. *Front. Cell. Infect. Microbiol.* **2020**, *10*, 591121. [[CrossRef](#)]

49. Frontiers | Antibody Responses Against Plasmodium Vivax TRAP Recombinant and Synthetic Antigens in Naturally Exposed Individuals From the Brazilian Amazon | Immunology. Available online: <https://www.frontiersin.org/articles/10.3389/fimmu.2019.02230/full> (accessed on 28 May 2022).
50. Campos, M.P.; Figueiredo, F.B.; Morgado, F.N.; dos Santos Renzetti, A.R.; de Souza, S.M.M.; Pereira, S.A.; Rodrigues-Da-Silva, R.N.; Lima-Junior, J.D.C.; De Luca, P.M. Leishmania Infantum Virulence Factor A2 Protein: Linear B-Cell Epitope Mapping and Identification of Three Main Linear B-Cell Epitopes in Vaccinated and Naturally Infected Dogs. *Front. Immunol.* **2018**, *9*, 1690. [[CrossRef](#)]
51. Fontes, S.d.S.; Maia, F.d.M.; Ataide, L.S.; Conte, F.P.; Lima-Junior, J.d.C.; Rozental, T.; da Silva Assis, M.R.; Júnior, A.A.P.; Fernandes, J.; de Lemos, E.R.S.; et al. Identification of Immunogenic Linear B-Cell Epitopes in *C. Burnetii* Outer Membrane Proteins Using Immunoinformatics Approaches Reveals Potential Targets of Persistent Infections. *Pathogens* **2021**, *10*, 1250. [[CrossRef](#)]
52. Zargar, F.N.; Aky, A.; Rezaeian, S.; Ghadiri, K.; Lorestani, R.C.; Madanchi, H.; Safaei, S.; Rostamian, M. B Cell Epitopes of Four Fimbriae Antigens of Klebsiella Pneumoniae: A Comprehensive In Silico Study for Vaccine Development. *Int. J. Pept. Res. Ther.* **2021**, *27*, 875–886. [[CrossRef](#)]
53. Feodorova, V.A.; Lyapina, A.M.; Khizhnyakova, M.A.; Zaitsev, S.S.; Saltykov, Y.V.; Motin, V.L. Yersinia Pestis Antigen F1 but Not LcrV Induced Humoral and Cellular Immune Responses in Humans Immunized with Live Plague Vaccine—Comparison of Immunoinformatic and Immunological Approaches. *Vaccines* **2020**, *8*, 698. [[CrossRef](#)]
54. Kalkanlı Taş, S.; Kırkık, D.; Öztürk, K.; Tanoğlu, A. Determination of B- and T- Cell Epitopes for Helicobacter Pylori CagPAI: An in Silico Approach. *Turk. J. Gastroenterol.* **2020**, *31*, 713–720. [[CrossRef](#)] [[PubMed](#)]
55. Zhao, D.; Han, K.; Huang, X.; Zhang, L.; Wang, H.; Liu, N.; Tian, Y.; Liu, Q.; Yang, J.; Liu, Y.; et al. Screening and Identification of B-Cell Epitopes within Envelope Protein of Tembusu Virus. *Virol. J.* **2018**, *15*, 142. [[CrossRef](#)] [[PubMed](#)]
56. Palanisamy, N.; Lennerstrand, J. Computational Prediction of Usutu Virus E Protein B Cell and T Cell Epitopes for Potential Vaccine Development. *Scand. J. Immunol.* **2017**, *85*, 350–364. [[CrossRef](#)]
57. Nadugala, M.N.; Premaratne, P.H.; Goonasekara, C.L. Systematic Bioinformatic Approach for Prediction of Linear B-Cell Epitopes on Dengue E and PrM Protein. *Adv. Bioinforma.* **2016**, *2016*, 1–16. [[CrossRef](#)] [[PubMed](#)]
58. Tabrejee, S.; Hossain, M.M. In Silico Approach To Design a B-Cell Epitope Based Vaccine Target Against Yellow Fever Virus. *Bangladesh J. Microbiol.* **2018**, *35*, 27–35. [[CrossRef](#)]
59. Slathia, P.S.; Sharma, P. A Common Conserved Peptide Harboring Predicted T and B Cell Epitopes in Domain III of Envelope Protein of Japanese Encephalitis Virus and West Nile Virus for Potential Use in Epitope Based Vaccines. *Comp. Immunol. Microbiol. Infect. Dis.* **2019**, *65*, 238–245. [[CrossRef](#)]
60. Amrun, S.N.; Yee, W.-X.; Abu Bakar, F.; Lee, B.; Kam, Y.-W.; Lum, F.-M.; Tan, J.J.; Lim, V.W.; Watthanaworawit, W.; Ling, C.; et al. Novel Differential Linear B-Cell Epitopes to Identify Zika and Dengue Virus Infections in Patients. *Clin. Transl. Immunol.* **2019**, *8*, e1066. [[CrossRef](#)]
61. Freire, M.C.L.C.; Pol-Fachin, L.; Coêlho, D.F.; Viana, I.F.T.; Magalhães, T.; Cordeiro, M.T.; Fischer, N.; Loeffler, F.F.; Jaenisch, T.; Franca, R.F.; et al. Mapping Putative B-Cell Zika Virus NS1 Epitopes Provides Molecular Basis for Anti-NS1 Antibody Discrimination between Zika and Dengue Viruses. *ACS Omega* **2017**, *2*, 3913–3920. [[CrossRef](#)]
62. Manikandan, M.; Prabu, S.; Rajeswari, K.; Kamaraj, R.; Krishnan, S. In Silico Prediction of B-Cell Epitopes of Dengue Virus—A Reverse Vaccinology Approach. *J. Appl. Pharm. Sci.* **2020**, *10*, 77–85. [[CrossRef](#)]
63. Biering, S.B.; Akey, D.L.; Wong, M.P.; Brown, W.C.; Lo, N.T.N.; Puerta-Guardo, H.; Tramontini Gomes de Sousa, F.; Wang, C.; Konwerski, J.R.; Espinosa, D.A.; et al. Structural Basis for Antibody Inhibition of Flavivirus NS1–Triggered Endothelial Dysfunction. *Science* **2021**, *371*, 194–200. [[CrossRef](#)]
64. Chung, K.M.; Nybakken, G.E.; Thompson, B.S.; Engle, M.J.; Marri, A.; Fremont, D.H.; Diamond, M.S. Antibodies against West Nile Virus Nonstructural Protein NS1 Prevent Lethal Infection through Fc γ Receptor-Dependent and -Independent Mechanisms. *J. Virol.* **2006**, *80*, 1340–1351. [[CrossRef](#)] [[PubMed](#)]
65. Wessel, A.W.; Kose, N.; Bombardi, R.G.; Roy, V.; Chantima, W.; Mongkolsapaya, J.; Edeling, M.A.; Nelson, C.A.; Bosch, I.; Alter, G.; et al. Antibodies Targeting Epitopes on the Cell-Surface Form of NS1 Protect against Zika Virus Infection during Pregnancy. *Nat. Commun.* **2020**, *11*, 5278. [[CrossRef](#)] [[PubMed](#)]
66. Akey, D.L.; Brown, W.C.; Dutta, S.; Konwerski, J.; Jose, J.; Jurkiw, T.J.; DelProposto, J.; Ogata, C.M.; Skiniotis, G.; Kuhn, R.J.; et al. Flavivirus NS1 Structures Reveal Surfaces for Associations with Membranes and the Immune System. *Science* **2014**, *343*, 881–885. [[CrossRef](#)]
67. Akey, D.L.; Brown, W.C.; Jose, J.; Kuhn, R.J.; Smith, J.L. Structure-Guided Insights on the Role of NS1 in Flavivirus Infection. *BioEssays* **2015**, *37*, 489–494. [[CrossRef](#)] [[PubMed](#)]
68. Nair, D.T.; Singh, K.; Siddiqui, Z.; Nayak, B.P.; Rao, K.V.S.; Salunke, D.M. Epitope Recognition by Diverse Antibodies Suggests Conformational Convergence in an Antibody Response. *J. Immunol.* **2002**, *168*, 2371–2382. [[CrossRef](#)]
69. Influence of Protein Flexibility and Peptide Conformation on Reactivity of Monoclonal Anti-Peptide Antibodies with a Protein Alpha-Helix. | PNAS. Available online: <https://www.pnas.org/doi/abs/10.1073/pnas.84.23.8568> (accessed on 25 May 2022).
70. Prediction of Protein Antigenic Determinants from Amino Acid Sequences. | PNAS. Available online: https://www.pnas.org/doi/10.1073/pnas.78.6.3824?url_ver=Z39.88-2003&rfr_id=ori:rid:crossref.org&rfr_dat=cr_pub%20%200pubmed (accessed on 25 May 2022).

71. Kyte, J.; Doolittle, R.F. A Simple Method for Displaying the Hydropathic Character of a Protein. *J. Mol. Biol.* **1982**, *157*, 105–132. [[CrossRef](#)]
72. Parker, J.M.R.; Guo, D.; Hodges, R.S. New Hydrophilicity Scale Derived from High-Performance Liquid Chromatography Peptide Retention Data: Correlation of Predicted Surface Residues with Antigenicity and x-Ray-Derived Accessible Sites. *Biochemistry* **1986**, *25*, 5425–5432. [[CrossRef](#)]
73. Emini, E.A.; Hughes, J.V.; Perlow, D.S.; Boger, J. Induction of Hepatitis A Virus-Neutralizing Antibody by a Virus-Specific Synthetic Peptide. *J. Virol.* **1985**, *55*, 836–839. [[CrossRef](#)]
74. Karplus, P.A.; Schulz, G.E. Prediction of Chain Flexibility in Proteins. *Naturwissenschaften* **1985**, *72*, 212–213. [[CrossRef](#)]
75. B-Cell Epitopes (DNASTAR)-User Guide to Protean 3D-17.2. Available online: <https://www.dnastar.com/manuals/protean3d/17.2/en/topic/b-cell-epitopes-neoclone> (accessed on 25 May 2022).
76. Ponomarenko, J.; Bui, H.-H.; Li, W.; Fusseder, N.; Bourne, P.E.; Sette, A.; Peters, B. ElliPro: A New Structure-Based Tool for the Prediction of Antibody Epitopes. *BMC Bioinformatics* **2008**, *9*, 514. [[CrossRef](#)]
77. Doytchinova, I.A.; Flower, D.R. Vaxijen: A Server for Prediction of Protective Antigens, Tumour Antigens and Subunit Vaccines. *BMC Bioinformatics* **2007**, *8*, 4. [[CrossRef](#)] [[PubMed](#)]
78. Frontiers | Antigenic Peptide Prediction From E6 and E7 Oncoproteins of HPV Types 16 and 18 for Therapeutic Vaccine Design Using Immunoinformatics and MD Simulation Analysis | Immunology. Available online: <https://www.frontiersin.org/articles/10.3389/fimmu.2018.03000/full> (accessed on 25 May 2022).
79. Gasteiger, E.; Hoogland, C.; Gattiker, A.; Duvaud, S.; Wilkins, M.R.; Appel, R.D.; Bairoch, A. Protein Identification and Analysis Tools on the ExPASy Server. In *The Proteomics Protocols Handbook*; Walker, J.M., Ed.; Humana Press: Totowa, NJ, USA, 2005; pp. 571–607. ISBN 978-1-58829-343-5.
80. Yang, J.; Zhang, Y. I-TASSER Server: New Development for Protein Structure and Function Predictions. *Nucleic Acids Res.* **2015**, *43*, 174–181. [[CrossRef](#)] [[PubMed](#)]
81. Tovchigrechko, A.; Vakser, I.A. GRAMM-X Public Web Server for Protein–Protein Docking. *Nucleic Acids Res.* **2006**, *34*, W310–W314. [[CrossRef](#)] [[PubMed](#)]
82. Song, H.; Qi, J.; Haywood, J.; Shi, Y.; Gao, G.F. Zika Virus NS1 Structure Reveals Diversity of Electrostatic Surfaces among Flaviviruses. *Nat. Struct. Mol. Biol.* **2016**, *23*, 456–458. [[CrossRef](#)]
83. Olsson, M.H.M.; Søndergaard, C.R.; Rostkowski, M.; Jensen, J.H. PROPKA3: Consistent Treatment of Internal and Surface Residues in Empirical pK_a Predictions. *J. Chem. Theory Comput.* **2011**, *7*, 525–537. [[CrossRef](#)]
84. Abraham, M.J.; Murtola, T.; Schulz, R.; Páll, S.; Smith, J.C.; Hess, B.; Lindahl, E. GROMACS: High Performance Molecular Simulations through Multi-Level Parallelism from Laptops to Supercomputers. *SoftwareX* **2015**, *1–2*, 19–25. [[CrossRef](#)]
85. Hess, B.; Bekker, H.; Berendsen, H.J.C.; Fraaije, J.G.E.M. LINCS: A Linear Constraint Solver for Molecular Simulations. *J. Comput. Chem.* **1997**, *18*, 1463–1472. [[CrossRef](#)]
86. Miyamoto, S.; Kollman, P.A. Settle: An Analytical Version of the SHAKE and RATTLE Algorithm for Rigid Water Models. *J. Comput. Chem.* **1992**, *13*, 952–962. [[CrossRef](#)]
87. Berendsen, H.J.C.; Postma, J.P.M.; van Gunsteren, W.F.; DiNola, A.; Haak, J.R. Molecular Dynamics with Coupling to an External Bath. *J. Chem. Phys.* **1984**, *81*, 3684–3690. [[CrossRef](#)]
88. Hutter, J. Car-Parrinello Molecular Dynamics: Car-Parrinello Molecular Dynamics. *Wiley Interdiscip. Rev. Comput. Mol. Sci.* **2012**, *2*, 604–612. [[CrossRef](#)]
89. Hockney, R.W.; Goel, S.P.; Eastwood, J.W. Quiet High-Resolution Computer Models of a Plasma. *J. Comput. Phys.* **1974**, *14*, 148–158. [[CrossRef](#)]
90. Daura, X.; Gademann, K.; Jaun, B.; Seebach, D.; van Gunsteren, W.F.; Mark, A.E. Peptide Folding: When Simulation Meets Experiment. *Angew. Chem. Int. Ed.* **1999**, *38*, 236–240. [[CrossRef](#)]
91. Pettersen, E.F.; Goddard, T.D.; Huang, C.C.; Couch, G.S.; Greenblatt, D.M.; Meng, E.C.; Ferrin, T.E. UCSF Chimera—a Visualization System for Exploratory Research and Analysis. *J. Comput. Chem.* **2004**, *25*, 1605–1612. [[CrossRef](#)] [[PubMed](#)]
92. Pettersen, E.F.; Goddard, T.D.; Huang, C.C.; Meng, E.C.; Couch, G.S.; Croll, T.I.; Morris, J.H.; Ferrin, T.E. UCSF CHIMERAX: Structure Visualization for Researchers, Educators, and Developers. *Protein Sci.* **2021**, *30*, 70–82. [[CrossRef](#)]
93. Rodrigues, R.L.; Menezes, G.D.L.; Saivish, M.V.; Costa, V.G.D.; Pereira, M.; Moreli, M.L.; Silva, R.A.D. Prediction of MAYV Peptide Antigens for Immunodiagnostic Tests by Immunoinformatics and Molecular Dynamics Simulations. *Sci. Rep.* **2019**, *9*, 13339. [[CrossRef](#)]